ELSEVIER

Polymer Vol. 37 No. 15, pp. 3303–3311, 1996

Printed in Great Britain
0032-3861/96/$15.00 + 0.00

Characterization of strain-induced crystallization of poly(ethylene terephthalate) at fast draw rates using synchrotron radiation

D. J. Blundell and D. H. MacKerron
ICI Films, PO Box No. 90, Wilton Research Centre, Middlesbrough, Cleveland TS90 8JE, UK

W. Fuller*, A. Mahendrasingam and C. Martin
Department of Physics, Keele University, Staffordshire ST5 5BG, UK

R. J. Oldman and R. J. Rule
ICI Chemicals and Polymers Ltd, Runcorn Technical Centre, Runcorn, Cheshire WA7 4QD, UK

and C. Riekel
ESRF, BP 220, F-38043 Grenoble Cedex, France
(Received 4 September 1995; revised 6 October 1995)

Structural changes during fast drawing of poly(ethylene terephthalate) were studied by wide-angle X-ray scattering using synchrotron radiation. Drawing was studied at 80, 90, 100 and 110°C to a final draw ratio of ~4:1 at a draw rate of ~ $10\,s^{-1}$. Simultaneous video recording of the sample enabled variation in the X-ray pattern to be correlated with local extension. Essentially all oriented crystallization occurred after final extension. Primary crystallization fits a first-order transformation with little change in the rate of crystallization observed over the 30°C range of temperature. These results show that it can be misleading to rely on crystallinity information obtained when samples from interrupted draw experiments are quenched.

(Keywords: poly(ethylene terephthalate); crystallization kinetics; X-ray synchrotron radiation)

INTRODUCTION

One of the most challenging issues in the crystallization of polymers is the nature and kinetics of the strain-induced crystallization that takes place when polymers such as poly(ethylene terephthalate) (PET) are mechanically drawn close to the glass transition temperature (T_g). In this paper recent results using the European Synchrotron Radiation Facility (ESRF) are reported, from which it has been possible to monitor crystallization in real time when amorphous PET was drawn at fast rates that are comparable to those used in industrial processing.

Most previous detailed studies of strain-induced crystallization have been carried out on flexible polymers such as natural rubbers that have a permanently cross-linked network[1–3]. For these materials it was shown that, when the network is uniaxially extended from the unoriented state, there is a change in the crystallization process from one that involves the growth of three-dimensional units such as spherulites towards kinetics associated with a first-order transition. It is not easy to reproduce these types of experiments in PET where there are no permanent crosslinks and where crystallization on drawing near T_g is very much faster[4].

When the entangled molecular network of PET is extended there is competition between, on the one hand, the relaxation of the network, leading to disorientation and, on the other hand, crystallization, which effectively crosslinks the network to prevent disorientation. The final orientation attained in a sample for a given draw ratio will depend on the relative effectiveness of these processes. Higher draw ratios will increase the entropic driving force of the relaxation but will also increase the rate of strain-induced crystallization. Higher temperatures will increase the segmental mobility, which will promote both relaxation and crystallization. Although there is therefore much interest in the interplay between these processes, it is difficult to obtain experimental data, not least because of the very fast rate at which strain-induced crystallization occurs. At low draw ratios before the onset of crystallization, several studies have been able to interpret the orientation in terms of models based on the deformation of an entangled network[5–8]. At or just above the T_g the network can to a first approximation be considered as a simple rubber network with a crosslink

* To whom correspondence should be addressed

density depending on the temperature and draw rate. At higher draw ratios deviations from this simplified behaviour occur and can often be attributed to chain slippage or strain-induced crystallization modifying the effective network[7,8]. Attempts to quantify crystallization as a function of draw ratio usually rely on interrupting the draw and then quenching the samples in an attempt to freeze in the structure so that it can be characterized at room temperature. In a systematic study of this kind Salem[9] has proposed that characteristic points on the stress–strain curve can be ascribed to the onset of a rapid crystallization regime followed by a second slower crystallization regime.

There are difficulties in studies of this type, particularly for fast drawing rates. First, it is necessary to make the assumption that there is no change in the structure in the period between the end of the extension and quenching below T_g. Secondly, one cannot assume that results and observations obtained at low draw rates extrapolate to the high rates commonly used in industrial processes. At low rates, where the crystallization is fast compared with the timescale of drawing, there is a greater chance that crystallization will occur during the drawing process and will be able to reinforce the orientation while the sample is still being draw. At fast rates it is possible that the same degree of draw could be achieved before crystallization occurs. The work reported here overcomes these difficulties. The variation in the X-ray diffraction pattern has been observed in real time throughout the complete drawing process, thus avoiding the need to quench the sample. This has been carried out at draw rates of $\sim 10\,s^{-1}$, which is significantly faster than in previous studies[10]. The ability to do this depends on a combination of an ESRF beamline using an undulator as radiation source to produce a small and well collimated beam and the availability of a two-dimensional CCD (charge-coupled device) detector in a system capable of fast data transfer. Experiments are described in which strips of amorphous PET film were drawn at four temperatures (80, 90, 100 and 110°C) to a fixed nominal draw ratio of 4:1. An analysis of the two-dimensional diffraction patterns enables the point of crystallization to be observed and also gives important new information on the kinetics of the crystallization process.

EXPERIMENTAL

The specimens of PET were strips approximately 1 cm long and 1 cm wide cut from a sheet of cast film $\sim 840\,\mu m$ thick. The X-ray camera was purpose designed and constructed in the Keele Physics Department workshops[11]. It consisted of a 150 mm × 150 mm × 150 mm oven of which three sides were interchangeable so that it was possible to exchange sides depending on the particular application. This allowed the viewing port in which the video camera was mounted to be varied according to the overall size and shape of the specimen being studied. The oven was heated electrically by elements mounted on the top and bottom of its interior and the temperature throughout the oven was kept uniform by the use of an air circulating fan. The temperature of the oven could be controlled to within 1°C and the maximum temperature attainable was 350°C. Air at normal pressure within the camera allowed better control of the specimen temperature than would have been achieved with an evacuated camera or one that was continuously flushed with helium. X-ray background scatter from the air was insignificant in the region of the diffraction data used in this analysis. The sample of PET was clamped between two jaws attached to stepper motors, which allowed uniaxial bidirectional drawing at rates up to $12\,s^{-1}$.

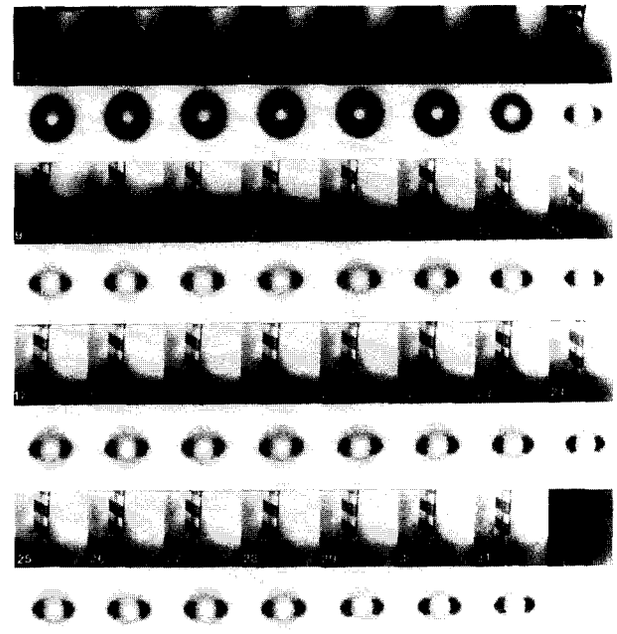

Figure 1 X-ray diffraction patterns with corresponding video image of sample recorded during drawing at 90°C. Each of the 31 frames was recorded with an exposure time of 40 ms. There was essentially no dead-time between frames, so that the drawing experiment was completed in ~ 1.2 s

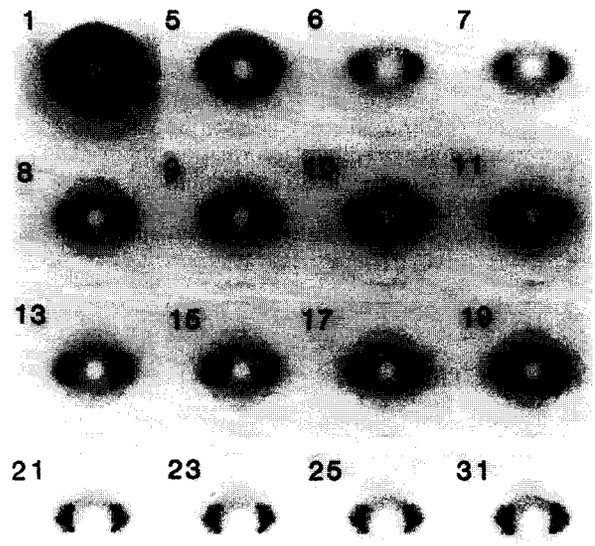

Figure 2 X-ray diffraction frames (with frame number) selected from the 31 frames recorded during drawing at 80°C

WAXS data were recorded on the SAXS endstation of the Microfocus beamline ID13 at the ESRF[12]. The mirror/monochromator optics produced a highly collimated beam of $\sim 150\,\mu m$ diameter at the specimen with a wavelength of 0.92 Å and a flux of $\sim 5 \times 10^{11}$ photons s^{-1}. Diffraction patterns were recorded using a

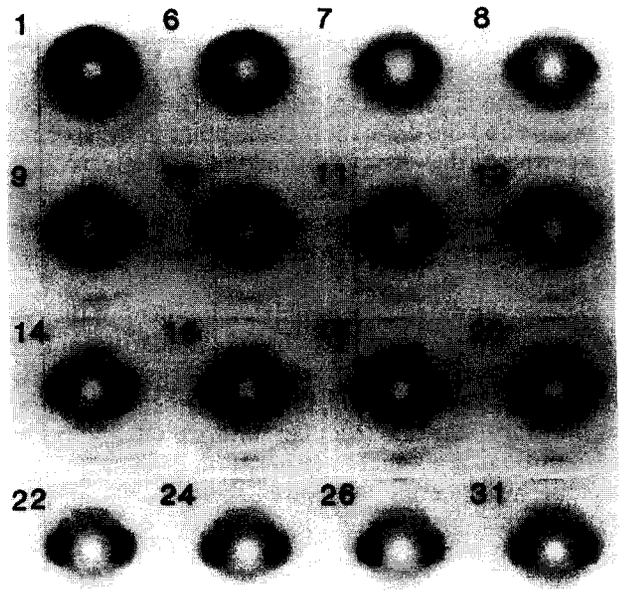

Figure 3 X-ray diffraction frames (with frame number) selected from the 31 frames recorded during drawing at 90°C

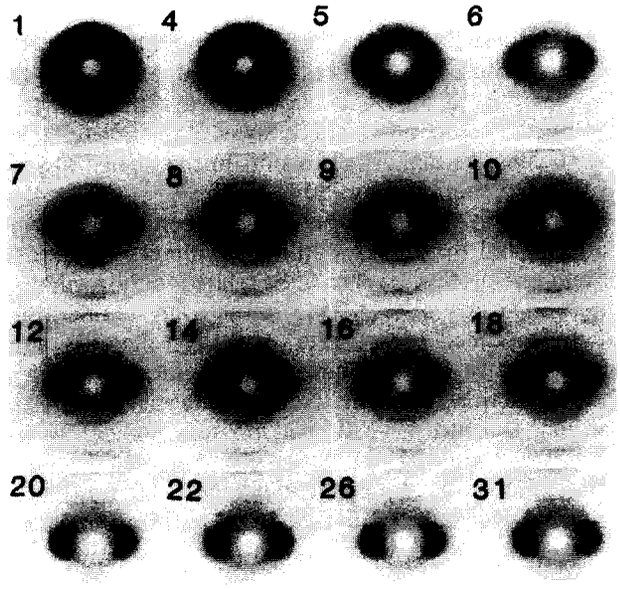

Figure 4 X-ray diffraction frames (with frame number) selected from the 31 frames recorded during drawing at 100°C

Photonics Science CCD detector with a sensitive area of 92 mm × 69 mm and an effective pixel area of 120 μm × 120 μm. The specimen-to-detector distance could be as small as 6 cm. Diffraction patterns were recorded with exposure times of 40 ms. Over this period, the pattern was accumulated within the detector before being digitized by a Synoptic i860 framegrabber within an eight-bit word. By accumulating diffraction patterns from the same specimen over different exposure times, we confirmed that for the conditions of our experiments the detector response was linear. For the wavelength of the X-rays used in these experiments and the thickness of the specimens, absorption corrections were insignificant. Thirty-one frames could be recorded 'end-to-end' with essentially no dead-time between frames before the memory of the framegrabber was full. At this stage

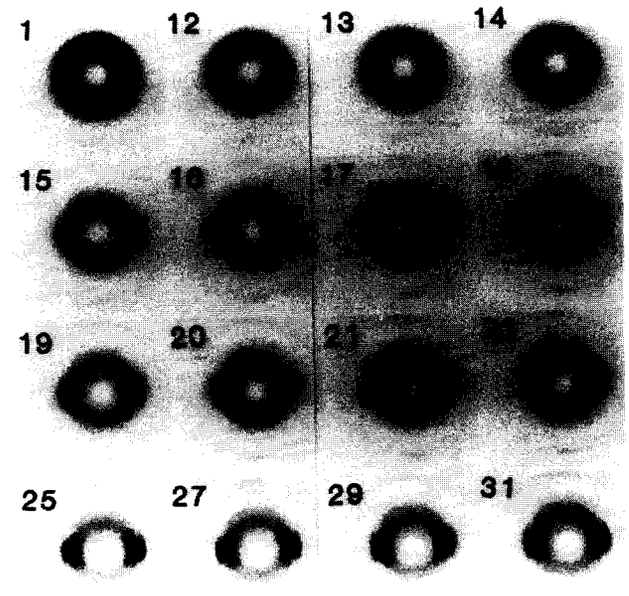

Figure 5 X-ray diffraction frames (with frame number) selected from the 31 frames recorded during drawing at 110°C

these frames were downloaded through an SCSI interface to a 486 PC. In parallel with the transfer of data to the framegrabber, the signal accumulated in the CCD during each 40 ms was written to a standard video cassette recorded using VHS format. Although data recorded on video tape have limitations for accurate determination of structure factor amplitudes in a detailed X-ray structural refinement, the video recorded image is more than adequate for monitoring variation in orientation and crystallinity and has the advantage of providing a display in real time which monitors the variation in the diffraction pattern with the standard 25 Hz time resolution of a TV display. Video camera measurements on changes in the position of reference marks on the specimen at the region of the specimen from where the diffraction pattern was recorded allowed the precise draw ratio and draw rate to be calculated.

RESULTS

In time-resolved experiments of this kind involving multiple two-dimensional patterns and the corresponding TV images, an enormous quantity of diffraction data are generated, i.e. ~ 31 Mb in an experiment lasting 1.2 s. There is a major problem in condensing the data to a form that can be scrutinized so that selected data can be analysed in more detail. Software routines have therefore been developed to display both the TV and X-ray diffraction data from one whole experiment on one image. An example for one full set of data is shown in *Figure 1* for drawing at 90°C. In order to present more fully the variation in the diffraction pattern on which the analysis in this paper is based, selected frames are shown in *Figures 2, 3, 4* and *5* for each of the four experiments in which PET was drawn at 80, 90, 100 and 110°C respectively.

There are significant differences in the change in the dimensions of a PET film during drawing as a function of the draw temperature. At 90°C, there is a relatively short neck so that the effective draw at the point where the beam hits the sample occurs within the first two to three

Table 1 Summary of drawing conditions. The table shows the draw rate and draw ratio at the region of the specimen from which the X-ray diffraction pattern was recorded. These values were calculated from measurements on the change in position during drawing of graduations on the specimen

Draw temperature (°C)	Mean draw rate (s^{-1})	Final draw ratio	Crystallinity from density (vol%)
80	40	4.5	30
90	20	4.2	26
100	10	3.8	27
110	10	3.8	29

Figure 6 Final diffraction pattern (i.e. frame 31) for sequence of patterns recorded during drawing at (a) 80°C and (b) 110°C

frames of the X-ray data. With increasing temperature, the development of the neck becomes progressively more gradual, so that by 110°C the drawing process is almost uniform along the sample length. The instantaneous draw rate and the draw ratio at the point in the specimen from where the X-ray diffraction pattern is being recorded can be derived from the variation with time in the separation of the distance markers in the video image. This has been used to calculate the draw rates and the draw ratios in *Table 1*.

Despite the differences in the development of the neck during drawing, there are broad similarities in the development of the diffraction patterns at different draw temperatures. In all four experiments there is a progression, starting from an unoriented amorphous halo, through a gradual intensification of the halo at the equator, which eventually gives the diffuse equatorial spots characteristic of a highly oriented amorphous structure, with finally the appearance of sharp diffraction spots from a highly oriented crystalline phase. There are some variations in the details of the oriented crystalline pattern at the different temperatures. *Figure 6* shows the final frames at the two extreme temperatures in which the main PET crystalline reflections are indexed. The differences in the overall patterns can be explained from the well known tendency for the (1 0 0) crystal planes to align preferentially parallel to the plane of oriented film samples due to an element of sideways restraint[9,13,14]. The effect is more prevalent at lower temperatures where the stresses are higher and results in the virtual absence of the (1 0 0) reflection at 80°C.

A frame-by-frame comparison between the diffraction patterns and the corresponding TV images enables the development of the pattern to be related to the local draw rate and draw ratio. At the lower draw temperatures where the local draw rate is faster, there is some uncertainty in fully defining correspondence, owing to the diffraction patterns being averaged over 40 ms periods. Despite this it is still possible to identify the point where the local drawing has effectively finished. In *Figures 2, 3, 4* and *5* this point corresponds to frames 5, 8, 5 and 13 respectively. In each of these frames there is a hint of crystalline reflections superimposed on the diffuse equatorial spots and a possibility that the very beginning of crystallization occurred just before the final draw ratio was achieved. However, it is clear that in all cases there is a major intensification of the crystalline reflections in the subsequent frames. This observation leads to the important conclusion that at these fast draw rates a substantial amount of the crystallization occurs after the extension has been completed. Interestingly, this is similar to the situation reported by Mitchell and Meier[3] for rapidly stretched crosslinked natural rubber. These observations also illustrate the point that for fast draw rates it is misleading to rely on crystallinity information obtained from experiments based on quenching fast-drawn samples. It is also clear from these figures that there is the possibility of monitoring and quantifying the rate and kinetics of the crystallization process.

CHARACTERIZATION OF RELATIVE CRYSTALLINITY

The development of crystallinity seen in the two-dimensional patterns can be investigated further by

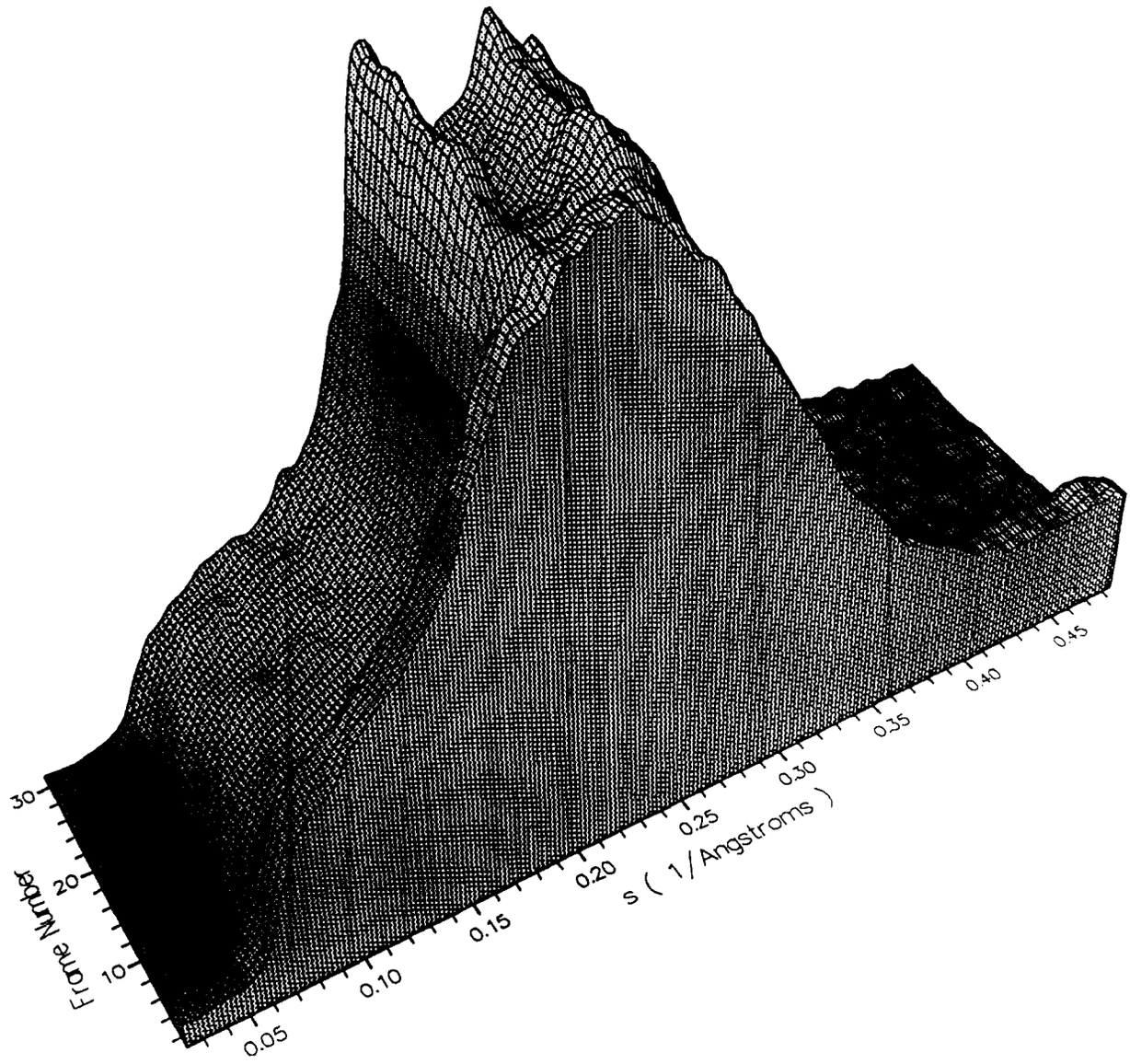

Figure 7 Variation of diffracted intensity across the equator of the diffraction pattern for the 31 frames recorded during drawing at 90°C

obtaining linear intensity profiles across the equator of the patterns. *Figure 7* shows an example of the 90°C case for which selected frames are in *Figure 3*, where the sharp crystalline peaks can be seen to emerge progressively above a diffuse background scatter. In the case of unoriented polymers it is a common practice to separate the scatter into crystalline and amorphous components in order to obtain a quantitative estimate of the crystallinity. This is not straightforward for the oriented patterns since it is necessary to use a profile for the background amorphous phase that is valid for the particular state of orientation of the amorphous phase. A decision was therefore made to use the profile of the amorphous phase taken from a frame just before the onset of crystallinity. *Figure 8* shows an example for the 90°C experiment in which the intensity profile of frame 8 of *Figure 3* has been scaled down slightly to fit the diffuse background of the subsequent frames and then subtracted to give a profile related to the crystalline component. The low residual of the difference on each side of the crystalline reflections demonstrates that the approach is reasonably valid. The areas under the crystalline peaks from such curves are shown plotted as a function of time in *Figure 9* for all four experiments. Time zero in these plots corresponds to the frame used for the amorphous profile and therefore occurs just before the finish of the draw but also before crystallinity is detected. Despite this all curves indicate a very sharp initial rise in crystallinity followed by a slower rise to an asymptotic value. The characteristic time to reach half of the final crystallinity is of the order of a tenth of a second, i.e. approaching three orders of magnitude faster than the maximum rate observed in unoriented PET.

Each of the sets of data plotted in *Figure 9* has been scaled by a different factor in order that the vertical scale of the plot gives a reasonable representation of the absolute crystallinity of the samples. Because of the differences in the preferential crystal alignment, one cannot directly derive crystallinities from the intensity distribution of the diffraction patterns. In order to derive the scaling factors, the densities of the final drawn sample from each experiment were measured for the region of the specimen from which the X-ray diffraction pattern was recorded. These densities were used to estimate the crystallinity assuming a simple two-phase model with a crystal density of $1.455\,g\,cm^{-3}$ and an amorphous density of $1.335\,g\,cm^{-3}$. The areas from each set were then scaled so as to make the area from the final frame

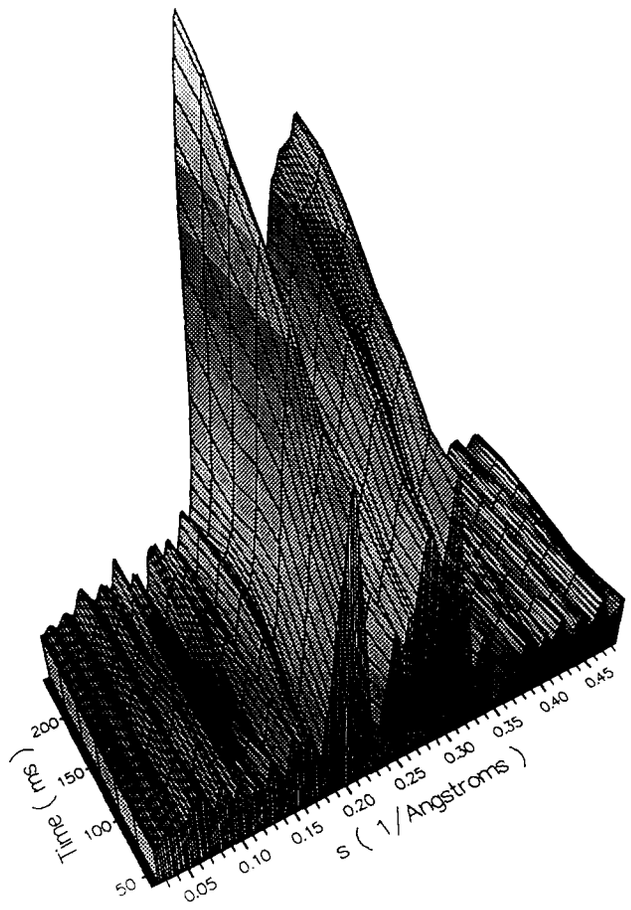

Figure 8 Development of crystalline peaks on the equator of the diffraction pattern after extension of the specimen had ceased (i.e. from frame 9 onwards) during drawing at 90°C. These diffraction profiles were obtained by subtracting the scaled equatorial scan of frame 8 from that of subsequent frames

equal to the estimated crystallinity. The estimated final levels of crystallinity are listed in *Table 1* and show little variation with temperature.

KINETICS OF CRYSTALLIZATION PROCESS

Despite the slight uncertainty in defining the end of the draw process and the start of crystallization, several pertinent observations can still be made on the nature of the kinetics of this crystallization process. An appropriate way to analyse the primary process is in terms of the Avrami equation[15]:

$$(\phi_\infty - \phi)/\phi_\infty = \exp(-kt^n) \qquad (1)$$

where ϕ_∞ represents the final attained crystallinity and ϕ is the crystallinity after time t from the start of the crystallization process. The parameter n is indicative of the type of crystallization process and can be estimated from the slope of the plot based on the logarithmic version of the Avrami equation:

$$\log\{-\ln[(\phi_\infty - \phi)/\phi_\infty]\} = n\log t + \log k \qquad (2)$$

This analysis has been applied to the above crystallinity estimates. As is often the case in unoriented crystallization, there is an indication of a secondary longer-term process taking over from the main primary process. Therefore various test values of ϕ_∞ were taken close to the final asymptotic value to establish reasonable linear Avrami relationships over the majority of the data points. Different trial values for ϕ_∞ had a negligible effect on the initial data points but did allow a choice where more points conformed to the main trend. The plots of the data are shown in *Figure 10*. The initial slopes of these plots are all close to unity. This is distinctly different from spherulitic crystallization from an unoriented melt where the value of n is usually close to 3.

It is interesting to note that a value of $n = 1$ is identical to that found in earlier studies of the crystallization of natural rubber that had been rapidly stretched to high draw ratios at low temperatures[1-3]. The straightforward interpretation in terms of the Avrami equation would be that the crystallization process is associated with the growth of entities in one dimension from pre-existing nuclei. This would conform to the model originally proposed by Flory[16] for fibrous crystal growth in the direction of strain.

However, the kinetics for $n = 1$ in equation (1) can also be regarded more generally as a first-order transformation process since this equation is in effect a solution to:

$$dA/dt = -kA \qquad (3)$$

where $A = (\phi_\infty - \phi)/\phi_\infty$ and where the rate of transformation is proportional to the amount of the disappearing phase. This is exemplified in *Figure 11* where, following equation (1), $\ln(\phi_\infty - \phi)/\phi_\infty$ is plotted against t. This is perhaps a more appropriate way of regarding the data and would be consistent with the sporadic appearance of uncorrelated crystals. This was also the conclusion of Kim and Mandelkern[2] in their studies of natural rubber where n was found to be equal to 1 and would fit the model proposed by Luch and Yeh[17].

The rate of crystallization is characterized by the parameter k, which is given by the slope in *Figure 11*. Despite the 30°C difference in draw temperatures, a similar value of around $10\,s^{-1}$ for the rate parameter is found for all four experiments. This is in clear distinction from crystallization from the unoriented melt, where the rate in the region just above T_g would be expected to vary by about three orders of magnitude over the same temperature range, owing to the large change in the transport term associated with main-chain motions[18]. It is possible that this insensitivity to temperature is due to two processes balancing out each other. For example, higher temperatures would increase the chain mobility and encourage the relaxation of chain orientation and hence reduce the driving force to crystallize but would also increase the chain motions involved in the crystallization process. An alternative possibility is that, irrespective of the temperature of draw, the chains in the oriented network are stretched beyond their natural degree of extension and are therefore slipping through entanglements. In order for the crystallization of these fully extended chains to take place, it may be sufficient to rely on chain movements associated with local segment reorientation where there is a relatively weak dependence on temperature. Such a process would also help to explain why the final levels of crystallinity recorded at different temperatures are similar. Therefore, significant main-chain motions associated with the glass

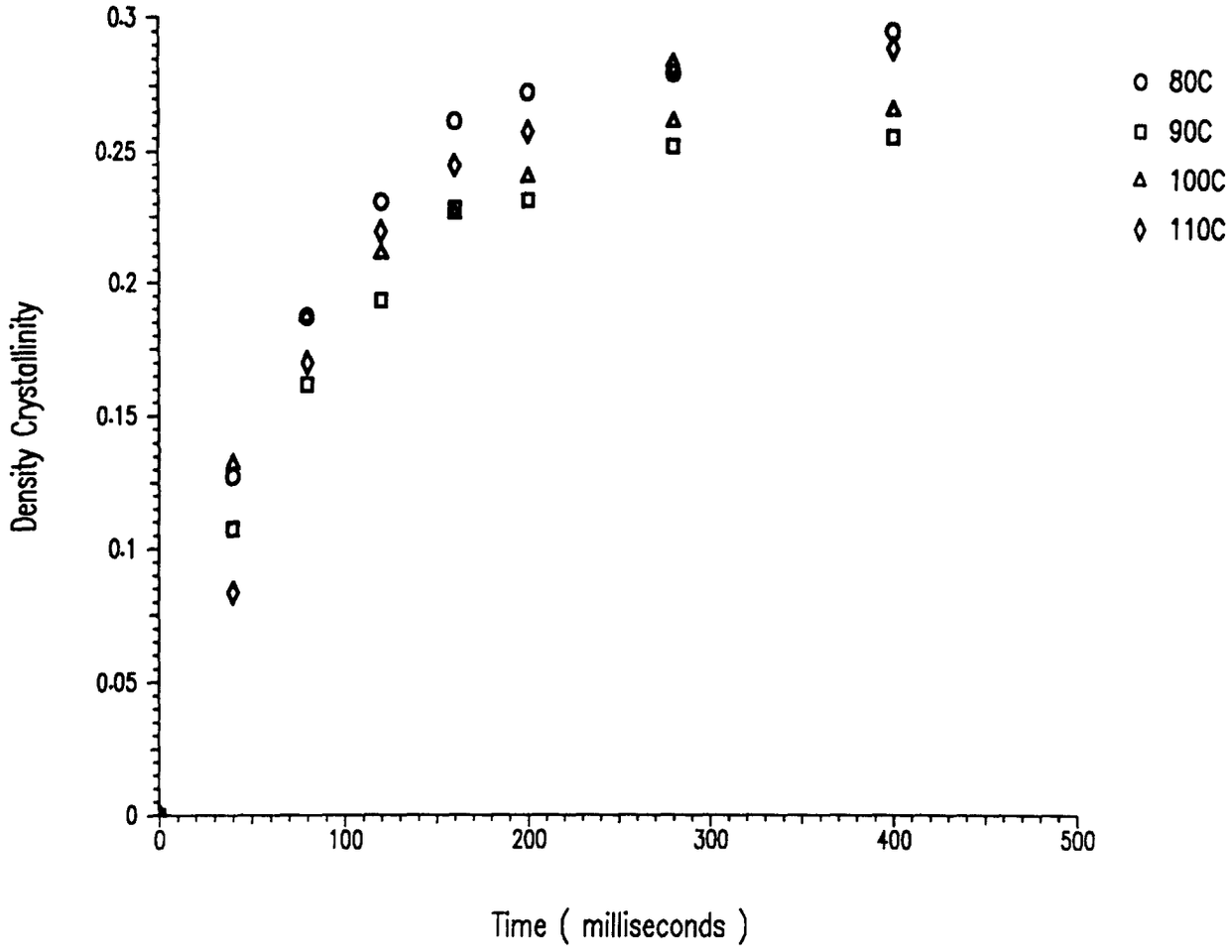

Figure 9 Estimated crystallinity as a function of time after extension had ceased during drawing at 80, 90, 100 and 110 C (i.e. respectively from frames, 6, 9, 6 and 14 onwards)

transition with their strong dependence on temperature may not be necessary to provide the mobility to enable sequences of monomer to move into crystallographic register. This scenario could also help to explain why crystallization does not start until after the extension process. The ability of local segments to provide the mobility for chains to organize into crystallographic register is likely to be restricted while extension and chain slippage are still in progress. However, when extension has been completed, the onset of chain relaxation would restore the freedom of local organization and allow crystal nucleation to occur.

The similarities with previous observations on highly stretched rubbers suggest that this form of kinetics is characteristic of crystallization from oriented polymers when a substantial fraction of the chain segments are fully extended. This would be distinct from the case of intermediate orientation where a small fraction of extended chains can lead to row nucleation and to a shish-kebab crystal morphology[19]. The above inferred sporadic appearance of uncorrelated crystals can be rationalized by a situation where nucleation occurs readily but where subsequent growth on the nuclei is severely retarded or suppressed. This could follow if the chains emanating from the crystals are entangled so as to frustrate further growth or if the constraint imposed on these chains by the crystals creates an effective rigid amorphous phase[20] at the boundary of the crystal nuclei.

Many of the aspects suggested by Luch and Yeh[17] in their model for the strain-induced crystallization of rubber are consistent with the present observations on PET. The curiosity in the current work is that, whereas the observations on rubber were made close to the crystal melting point of an inherently flexible chain, the PET is a less flexible polymer and the crystallization is occurring well below the crystal melting point and in the vicinity of T_g where main-chain motions are restricted.

TEMPERATURE VARIATIONS DURING DRAWING PROCESS

It is recognized that the process of drawing will generate heat and a rise in temperature. Calorimeter studies of the drawing of PET by Andrianova *et al.*[21] showed that heat generated of around $10\,J\,g^{-1}$ can occur at a draw ratio of 4. Most of this heat was shown to be associated with crystallization. If all this heat is retained within the sample, it would raise the temperature by about 5°C. However, this earlier work used low draw rates where crystallization started at a draw ratio of 2 and then continued to occur during the rest of the draw. At the high rates used in our experiments, the above analysis shows that crystallization occurs mainly after the draw has finished, so the main component of the heat generated will occur after this. The extent of any temperature rise will depend on how quickly this heat can be dissipated.

Simple heat-flow calculations have been made on the

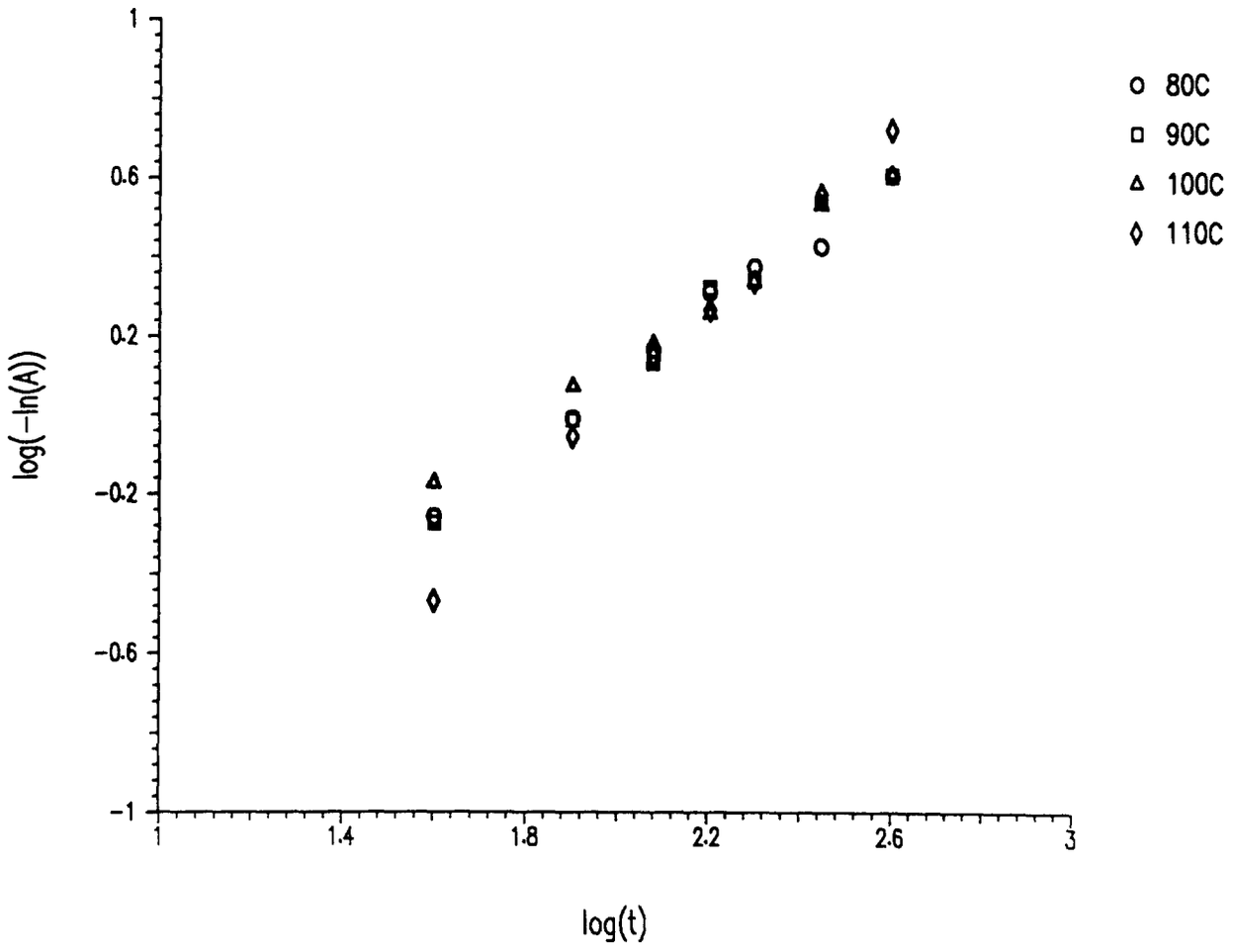

Figure 10 Avrami plot of $A = (\phi_\infty - \phi)/\phi_\infty$ against time t for drawing at 80, 90, 100 and 110°C (see equation (2))

basis of a heat transfer coefficient between the PET films and the surrounding circulating air of $100\,J\,m^{-2}\,K^{-1}$. This indicates that the flow of heat from the sample will occur with a characteristic time constant that would vary from about 5 s for a film of the initial thickness of 800 μm down to about 1 s for a film of the final drawn thickness of 200 μm. These temperature decay constants are longer than both the time of draw and the observed time of crystallization and indicate that the drawing and crystallization processes could be occurring in near-adiabatic conditions. It is probable therefore that the actual temperature of the sample will rise slightly during the drawing process and that this will be followed by a larger rise as crystallization proceeds. It is conceivable that the temperature effects could in fact have an autocatalytic action on the crystallization depending on how temperature influences the rate of crystallization.

Experiments are now being prepared to explore the effect of varying the draw ratio. If the crystallization rate is slower at lower draw ratios, the adiabatic effects may be alleviated.

CONCLUSIONS

The high intensity of the ESRF Microfocus beamline combined with a fast two-dimensional detector capable of displaying diffraction patterns in real time has enabled detailed information to be obtained on the structural changes that occur during the fast drawing of PET in conditions similar to those experienced in industrial drawing processes. The simultaneous video recording of the drawing sample has enabled the developing X-ray patterns to be correlated with the local state of extension of the polymer and its rate of development. In particular, this shows that at a final overall draw ratio of 4:1, with an overall draw rate of $10\,s^{-1}$, the oriented crystallization process takes place mainly after the final extension has been achieved.

The kinetics of this crystallization process have been followed by separating crystal reflections from the diffuse background scatter. The primary crystallization process appears to be a first-order process in which the crystallinity levels off exponentially with a rate constant of around $10\,s^{-1}$. This type of kinetics suggests that the strain-induced crystallization of PET is associated with the sporadic appearance of uncorrelated crystal entities. Surprisingly, unlike spherulitic crystallization, there is little change in the rate over a 30°C range of temperature. One possibility is that the faster crystallization expected from the increased molecular mobility at higher temperatures is compensated by greater relaxation of the orientation of the molecular network. Alternatively, the temperature insensitivity could be a characteristic of the mechanism of strain-induced crystallization whereby under such conditions crystallization only requires the mobility of local segments rather than the transport of the main-chain motions associated with the glass transition.

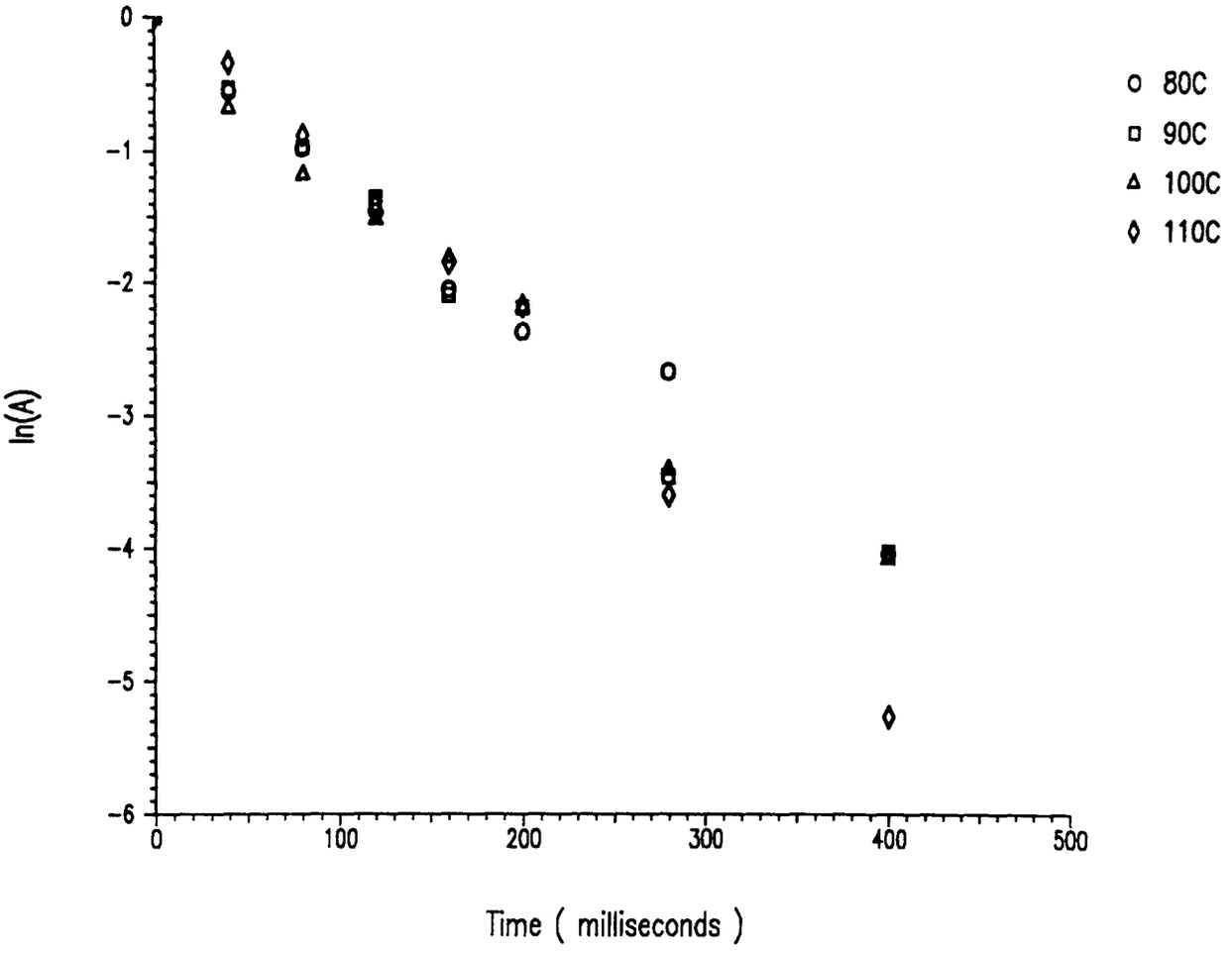

Figure 11 Plot of $A = (\phi_\infty - \phi)/\phi_\infty$ against time for drawing at 80, 90, 100 and 110°C

ACKNOWLEDGEMENTS

This work was supported by SERC Grant GR/H 67966 (to AM, WF, RJO and DJB) and allocations of beam time at the ESRF. We are grateful to P. J. Coleman, M. Daniels, M. G. Davies, G. Dudley, J. Gorini, E. J. T. Greasley, M. Lorenzen, G. Marsh, H. E. Moors, M. Wallace and P. Wattecamps for technical support and help with preparation of the manuscript.

REFERENCES

1 Gent, A. N. *Trans. Faraday Soc.* 1954, **50**, 521
2 Kim, H. and Mandelkern, L. *J. Polym. Sci. (A2)* 1968, **6**, 181
3 Mitchell, J. C. and Meier, D. J. *J. Polym. Sci. (A2)* 1968, **6**, 1689
4 Smith, F. S. and Steward, R. D. *Polymer* 1974, **15**, 283
5 Pinnock, P. R. and Ward, I. M. *Trans. Faraday Soc.* 1966, **62**, 1308
6 Cunningham, A., Ward, I. M., Willis, H. A. and Zichy, V. I. *Polymer* 1974, **15**, 749
7 Long, S. D and Ward, I. M. *J. Appl. Polym. Sci.* 1991, **42**, 1921
8 Perena, J. M., Ducket, R. A. and Ward, I. M. *J. Appl. Polym. Sci.* 1980, **25**, 1381
9 Salem, D. R. *Polymer* 1992, **33**, 3182
10 Salem, D. R. *Polymer* 1992, **33**, 3189
11 Mahendradingam, A., Fuller, W., Forsyth, V. T., Oldman, R. J., MacKerron, D. H. and Blundell, D. J. *Rev. Sci. Instrum.* 1992, **63**, 1087
12 Riekel, C., Bosecke, P., Diat, O., Lorenzen, M., Sanchez del Rio, M. and Snigireva, I. *Rev. Sci. Instrum.* 1995, **66**, 987
13 Casey, K. *Polymer* 1977, **18**, 1219
14 Bower, D. I., Jarvis, D. A. and Ward, I. M. *J. Polym. Sci. Phys.* 1986, **24**, 1459
15 Avrami, J. M. *J. Chem. Phys.* 1939, **2**, 1103; *ibid.* 1940, **8**, 212; *ibid.* 1941, **2**, 177
16 Flory, P. J. *J. Chem. Phys.* 1947, **15**, 397
17 Luch, D. and Yeh, G. S. Y. *J. Polym. Sci. (A2)* 1973, **11**, 467
18 Palys, L. H. and Phillips, P. J. *J. Polym. Sci.–Phys.* 1980, **18**, 829
19 Keller, A. and Machin, M. J. *J. Macromol. Sci.–Phys. (B)* 1967, **1**, 41
20 Menczel, J. and Wunderlich, B. *J. Polym. Sci., Polym. Lett. Edn.* 1981, **19**, 261
21 Andrianova, G. P., Popov, Y. V., Artamonova, S. D. and Arutyunov, B. A. *Vysokomol. Soyed. (A)* 1977, **19**, 1230